Offset-free Feedback Linearization Control of a Three-Phase Grid-connected Photovoltaic System

Rachid Errouissi, Ahmed Al-Durra, S. M. Muyeen.

Abstract: In this paper, a state feedback control law is combined with a disturbance observer to enhance disturbance rejection capability of a grid-connected photovoltaic inverter. The control law is based on input-output feedback linearization technique, while the existing disturbance observer is simplified and adopted for the system under investigation. The resulting control law has a PI/almost PID-like structure, which is convenient for real-time implementation. The objective of the proposed approach is to improve the dc-bus voltage regulation, while at the same time control the power exchange between the photovoltaic system and the grid. The stability of the closed-loop system under the composite controller is guaranteed by simple design parameters. Both simulation and experimental results show that the proposed method has significant abilities to initiate fast current control and accurate adjustment of the dc-bus voltage under model uncertainty and external disturbance.

1 Introduction

For a three-phase grid-connected photovoltaic system, the control objective is to maintain the DC-link voltage to a desired level, while at the same time regulating the reactive power of the grid [1]. Generally, the reactive power reference depends on whether the system operates under normal or voltage sag conditions [2]. In this work, only normal condition is considered, meaning that the grid-side converter should operate at unity power factor. The grid-connected PV inverter, with an output L-type filter, is a nonlinear multivariable system and subjected to unknown disturbances and model uncertainties [3]. For grid-connected inverter applications, linear controllers and classical PID controllers are well suited for improving steady-state performance if a small disturbance is considered around a known operating point [4]– [5]. However, such a performance may be guaranteed at the expense of degraded transient performance if the system works under severe operating condition, which results from the changes in atmospheric conditions. Several control techniques have been proposed to improve the reliability of the grid-connected PV system, including model predictive control [6], optimization-based PI controller [7], Lyapunov-based control [8], resonant current control [9], H_∞ control [10] etc. However, nonlinear control technique permits to obtain a stable and accurate control as it provides an opportunity for tighter guarantees on steady-state and transient performances [11]. Among these techniques, input-output feedback

R. Errouissi, A. Al-Durra and S. M. Muyeen are with the Petroleum Institute, P.O. Box 2533, Abu Dhabi, United Arab Emirates (e-mails: rerrouissi@pi.ac.ae, aaldurra@pi.ac.ae, and smmuyeen@pi.ac.ae).

linearization can be considered as a good candidate to initiate fast current control and accurate DC-link voltage regulation for a grid-connected inverter.

A look at the literature reveals that feedback linearization technique has been extensively studied for grid-connected inverter applications [12]–[20], and revealed that better performances can be obtained. In [18]– [19], a feedback linearization-based control has been applied to a grid-connected PV inverter system, where the switching actions of the power converter have been incorporated in the equation that describes the dynamics of the DC-link capacitor. Such a modeling approach offers the ability to deal with model uncertainty through the satisfaction of matching conditions. However, that leads to a partially linearized PV system, raising concern about the stability analysis of the internal dynamics. Such a concern has motivated the simplification of the equation that governs the dynamics of the DC-link capacitor, to ensure full linearization of the PV system via state feedback control law. As a result, there is no zero dynamics, and hence no additional stability analysis is required. The simplified model is derived by equaling the active power exchange between the ac grid and the dc-bus [21]. However, the major challenge in using this simplified approach lies in the presence of unmatched disturbance, i.e., the PV current, which should be decoupled from the system output to eliminate the steady-state error. Conventionally, an integral action is directly introduced in the loop to ensure offset-free feedback linearization. This strategy is commonly used for grid-connected inverter applications, but it may lead to undesirable transient performance if the integral time constant is not properly selected [20]. An alternative approach is to consider the information about the disturbance when designing a state feedback control law. Such a strategy, known as the exact disturbance decoupling (EDD), is still a challenging problem for nonlinear systems with unmatched disturbances, and has attracted a great deal of research, including those reported in [22]–[30]. The early attempts to improve the steady-state performance under unmatched disturbances were through the so-called almost disturbance decoupling technique, where the main objective was to guarantee input-to-state stability with respect to disturbance inputs [25]–[30]. An example of such an approach is the use of high gain controller [30], but this may cause the control effort to exceed its limiting value during the transient. These methods can attenuate the effect of the disturbances, but with the expense of a finite steady-state error. The limited accuracy of the available approaches has motivated the development of new techniques that can remove completely the steady-state error. A recent technique is the use of a disturbance observer based control [31]–[35]. Such a strategy is adopted in this paper to develop accurate and stable controller for a grid-connected PV system.

In a grid-connected PV system, the goal is to maintain the system output at a desired steady-state level, rather than tracking fast time-varying references. Moreover, the disturbance, caused by changes in atmospheric conditions, varies slowly. Driven by this observation, and following [31], EDD can be achieved by combining a state feedback control law with a disturbance observer. However, the design of such a disturbance observer is not trivial due to stability issue. On the other hand, the disturbance observer, proposed in [31], suffers from practical implementation difficulties that arise when a high-order nonlinear system model is integrated as a part of the composite controller. Therefore, in this work, a simplified disturbance observer is proposed and combined with a feedback linearization technique to control a grid-connected PV inverter with zero steady-state error. The composite controller is obtained by assuming that all states are available from direct measurement and have a constant steady-state response. Such an assumption is always valid for the system under investigation, meaning

that the proposed approach is feasible, and convenient for practical implementation. The only unknown variable is the PV current, but this can be produced by the disturbance observer. As a result, no additional current sensors are required to implement the proposed controller. The major advantage of the the proposed approach, compared to the existing methods, is that an integral action arises naturally in the composite controller rather than directly introducing it in the loop. Another promising feature is that the composite controller is equivalent to a PI/almost PID controller, which is easy to practically implement. The main contributions of this paper are summarized as follows

1) Design of an offset-free feedback linearization control of a three-phase grid-connected PV system to achieve exact disturbance decoupling under the presence of unmatched disturbance. Here, the physical unmatched disturbance is referred to the PV current i_0 as shown in Fig. 1.
2) No information about the current i_0 is required to practically implement to proposed controller. It is noticed that the current i_0 has a pulsating dc waveform because of the topology of the boost converter.
3) The nominal tracking performance can be achieved by choosing an adequate reference so that the current does not exceed its maximal value during transients, while the disturbance rejection performance can be specified by an appropriate tuning of the observer gain.
4) Unlike the existing disturbance observer-based control (DOBC) for systems with unmatched disturbance [31]–[35], the composite controller has a relatively simple structure, which makes it more convenient for real-time implementation. In other words, the integration of the system model is not considered as a part of controller.
5) Unlike the existing PV control technique inspired form the feedback linearization approach [20], no additional term is required to improve the transient performance at the startup phase. More specifically, only a smooth reference is required to achieve a good tracking performance during the transients.

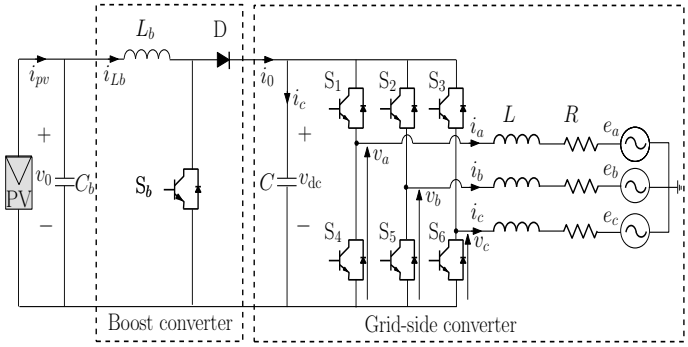

Fig. 1 Schematic diagram of a grid-connected photovoltaic inverter system.

2 Three phase grid-connected photovoltaic system modeling

The topology of the complete grid-connected PV inverter is depicted in Fig. 1. The PV output voltage v_0 is regulated by controlling the switching devise S_b of the boost converter, while the DC-link voltage v_{dc} is adjusted

through the switching actions of the inverter. C_b, L_b, C, L, R, represent, respectively, the input capacitor, the boost inductor, the DC-link capacitor, the filter inductor, and the filter resistor. The control of the grid-side converter represents the main concern of this study. Following [21], the equations that describe the dynamics of the DC-link capacitor and the filter current, in the dq reference frame, can be written as follows

$$\begin{cases} \frac{di_d}{dt} = -\frac{R}{L}i_d + \omega i_q + \frac{1}{L}v_d - \frac{1}{L}e_d \\ \frac{di_q}{dt} = -\frac{R}{L}i_q - \omega i_d + \frac{1}{L}v_q \\ \frac{dv_{dc}}{dt} = -\frac{3e_d}{2Cv_{dc}}i_d + \frac{i_0}{C} \end{cases} \tag{1}$$

where, i_d, i_q, and e_d, are respectively, d-axis current, q-axis current, and d-axis component of the grid voltage. The control signals v_d and v_q are the d-axis and the q-axis components of the inverter's output voltage. It is noted that such a model is obtained via $abc - dq$ transformation, for which the reference angle is provided by a phase-locked loop (PLL) algorithm. The PLL scheme is designed such that the q-axis component of the grid voltage e_q is maintained equal to zero. This can be done by using a simple PI controller [36], where the zero sequence components are ignored and the grid voltage is assumed to be balanced. The structure of the PLL is depicted in Fig. 2, where ω_0 represents the nominal angular frequency. Here, $\hat{\omega}$ and $\hat{\phi}$ are the estimation of the actual angular frequency ω and the angle ϕ for the synchronous reference frame, respectively. K_{pll} and T_{pll} represent, respectively, the proportional gain and the time constant of the PI controller. Such parameters can be obtained based, especially, on the specification of the settling time [36]. In this work, K_{pll} and T_{pll} are set, respectively, to 92 and 0.0217 s, so that the settling time is equal to 100 ms. In practice, the information

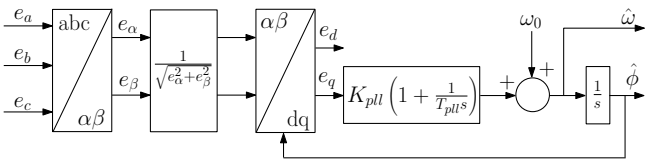

Fig. 2 Structure of The PLL

about i_0 is not always available for direct measurement and it varies with changes in atmospheric conditions. However, even if the pulsating current i_0 can be measurable, it cannot be directly used in the controller as it consists of a dc component and high frequency components due to the switching devise of the boost converter. More specifically, the current i_0 has a pulsating dc waveform. In addition, the model parameters cannot be accurately determined. Thus, in the presence of unknown external disturbance and parameter uncertainties, the above model can be rewritten as follows

$$\begin{cases} \frac{di_d}{dt} = -\frac{R}{L}i_d + \omega i_q + \frac{1}{L}v_d - \frac{1}{L}e_d + \frac{b_d}{L} \\ \frac{di_q}{dt} = -\frac{R}{L}i_q - \omega i_d + \frac{1}{L}v_q + \frac{b_q}{L} \\ \frac{dv_{dc}}{dt} = -\frac{3e_d}{2Cv_{dc}}i_d + \frac{b_v}{C} \end{cases} \tag{2}$$

where, b_d, b_q and b_v are additives variables that can represent model uncertainty, PV current variation, and PWM offset. In grid-connected photovoltaic system, the boost converter is usually used to achieve maximum power point. In such conditions, the PV current varies slowly compared to the dynamics of the system [20]. Moreover, by considering the slow changes in model parameters, one can assume that the disturbance $b(t)$ is

bounded. Moreover, by considering the slow changes in the PV power, it can be assumed that the dc component of i_0 is slow varying in comparison with the dynamics of the system. Therefore, the time derivative of $b(t)$ can be assumed to be around zero, in particular, as time goes to infinity. Hence, with the aim to simplify the design process and the stability analysis, one can assume that

$$\lim_{t\to\infty} \dot{b}\left(t\right) = 0 \tag{3}$$

3 Feedback linearization with a disturbance observer

3.1 Formulation of the control law

The main objective of state feedback control law, in this work, is to completely remove the effect of the disturbances in steady-state regime. The perturbed model of the three-phase grid-connected PV system (2) can be rearranged as follows

$$\begin{cases} \dot{x} = f\left(x\right) + g_1 u\left(t\right) + g_2 b\left(t\right) \\ y_i\left(t\right) = h_i\left(x\right), i = 1, 2 \end{cases} \tag{4}$$

where g_1 and g_2 are given by

$$g_1 = \begin{bmatrix} g_d & g_q \end{bmatrix} = \begin{bmatrix} \frac{1}{L} & 0 \\ 0 & \frac{1}{L} \\ 0 & 0 \end{bmatrix}, \; g_2 = \begin{bmatrix} \frac{1}{L} & 0 & 0 \\ 0 & \frac{1}{L} & 0 \\ 0 & 0 & \frac{1}{C} \end{bmatrix} \tag{5}$$

and $f(x)$ is defined as

$$f\left(x\right) = \begin{bmatrix} -\frac{R}{L} i_d + \omega i_q - \frac{e_d}{L} \\ -\frac{R}{L} i_q - \omega i_d \\ -\frac{3 e_d}{2 C v_{dc}} i_d \end{bmatrix} \tag{6}$$

The system output y and the input control u are given by

$$y = \begin{bmatrix} y_1 \\ y_2 \end{bmatrix} = \begin{bmatrix} i_q \\ v_{dc} \end{bmatrix}, \; u = \begin{bmatrix} v_d \\ v_q \end{bmatrix} \tag{7}$$

The state x and the disturbance b are defined as follows

$$x = \begin{bmatrix} i_d & i_q & v_{dc} \end{bmatrix}^T, \; b = \begin{bmatrix} b_d & b_q & b_v \end{bmatrix}^T \tag{8}$$

In the feedback linearization approach presented in [37], it is necessary to calculate the relative degree ρ_i with respect to the output y_i. Using the Lie derivative (see Appendix A), the first time derivative of y_1 is

$$\dot{y}_1\left(t\right) = L_f h_1\left(x\right) + L_{g_1} h_1\left(x\right) u + L_{g_2} h_1\left(x\right) b \tag{9}$$

As u appears in the first time derivative of y_1, then the relative degree ρ_1 is equal to 1. For the output y_2, we have

$$\begin{cases} \dot{y}_2\left(t\right) = L_f h_2\left(x\right) + L_{g_2} h_2\left(x\right) b \\ \ddot{y}_2\left(t\right) = L_f^2 h_2\left(x\right) + L_{g_1} L_f h_2\left(x\right) u + L_{g_2} L_f h_2\left(x\right) b + \frac{\dot{b}_v}{C} \end{cases} \tag{10}$$

Following (10), the relative degree ρ_2 is equal to 2. In addition, as the total relative degree $\rho = \rho_1 + \rho_2 = 3$, is equal to the system's order, then there is no zero dynamics [11]. It is worth noting that the states are available

for direct measurement. Therefore, the nonlinear system (4) is input-output feedback linearizable if the matrix G given below is nonsingular at least locally.

$$G\left(x\right)=\left[\begin{array}{c} L_{g_1}h_1\left(x\right) \\ L_{g_1}L_f h_2\left(x\right) \end{array}\right]=\left[\begin{array}{cc} 0 & \frac{1}{L} \\ -\frac{3e_d}{2LCv_{dc}} & 0 \end{array}\right] \tag{11}$$

Provided that, in practice, both v_{dc} and e_d cannot be equal to zero, the nonlinear system (4) is input-output feedback linearizable for the given output functions. The main result for the disturbance rejection ability using feedback linearization technique is stated in the following theorem.

Theorem 3.1. *Consider the nonlinear system (4) for the grid-connected PV inverter system, and suppose that the disturbance $b(t)$ and its time derivative are bounded and satisfy (3), then, the state feedback control law that guarantees zero steady-state error in the presence of both matched and unmatched disturbances is given by*

$$u=G^{-1}\left(x\right)\left(-\left[\begin{array}{c} L_f h_1\left(x\right) \\ L_f^2 h_2\left(x\right) \end{array}\right]-M\left(x\right)b+\left[\begin{array}{c} r_1 \\ r_2 \end{array}\right]\right) \tag{12}$$

where

$$M\left(x\right)=\left[\begin{array}{c} L_1\left(x\right) \\ L_2\left(x\right) \end{array}\right]=\left[\begin{array}{c} L_{g_2}h_1\left(x\right) \\ K_{12}L_{g_2}h_2\left(x\right)+L_{g_2}L_f h_2\left(x\right) \end{array}\right] \tag{13}$$

and

$$\left[\begin{array}{c} r_1 \\ r_2 \end{array}\right]=\left[\begin{array}{c} K_{01}e_1+\dot{y}_{r1} \\ K_{02}e_2+K_{12}\left(\dot{y}_{r2}-L_f h_2\left(x\right)\right)+\ddot{y}_{r2} \end{array}\right] \tag{14}$$

Here, $e_i=y_{ri}-y_i$ represents the tracking error and y_{ri} is the reference signal for the output y_i. The control gains K_{ji} are chosen such that the polynomials $P_1(s)$ and $P_2(s)$ given below are Hurwitz

$$P_1\left(s\right)=s+K_{01},\qquad P_2\left(s\right)=s^2+K_{12}s+K_{02} \tag{15}$$

Proof: Substituting (12) into (9) and (10), together with (13) and (14), leads to

$$\begin{cases} \dot{e}_1+K_{01}e_1=0 \\ \ddot{e}_2+K_{12}\dot{e}_2+K_{02}e_2=-\frac{\dot{b}_v}{C} \end{cases} \tag{16}$$

Since the polynomial $P_1(s)$ is Hurwitz, the tracking error e_1 converges to zero as time goes to infinity. With the assumption that $\dot{b}$ is bounded and the fact that the polynomial $P_2(s)$ is Hurwitz, one can show that the tracking error e_2 is bounded and its bound is proportional to that of $\dot{b}_v$ [37]. Furthermore, provided that $\dot{b}_v$ goes to zero as time goes to infinity, the output y_2 tracks its reference with an error which vanishes at steady-state regime. More specifically, the steady-state error will fluctuate around zero because of high frequency components associated with the current i_0. The control law (12) is still difficult to be implemented as the disturbance cannot be measured properly. As pointed in [30], the tracking problem for disturbed nonlinear systems can be solved without the need for the disturbance information by choosing the controller gains as follows

$$K_{01}=\frac{\alpha_{01}}{\varepsilon_i},\qquad K_{02}=\frac{\alpha_{02}}{\varepsilon_v^2},\qquad K_{12}=\frac{\alpha_{12}}{\varepsilon_v} \tag{17}$$

where $\varepsilon_{i,v}$ should be chosen sufficiently small, and α_{ij} are any chosen parameters such that the polynomials $Q_1(s)$ and $Q_2(s)$ given below are Hurwitz

$$Q_1 = s + \alpha_{01}, \qquad Q_2 = s^2 + \alpha_{12}s + \alpha_{02} \tag{18}$$

In this sutdy, the parameters α_{ij} are chosen as follows

$$\alpha_{01} = \frac{3}{2}, \quad \alpha_{02} = \frac{10}{3}, \quad \alpha_{12} = \frac{5}{2} \tag{19}$$

In fact, by reducing $\varepsilon_{i,v}$, we diminish the effect of the disturbance, which allows achieving better tracking performance with smaller steady-state error. This design procedure was adopted in [20] by choosing $\alpha_{01} = 1$, $\alpha_{02} = 1$, and $\alpha_{12} = 2$, where an integral action is directly introduced in the controller to eliminate completely the steady-state error caused by PV current variation. The major drawback of that method is that an additional term is required to avoid harsh behavior during startup phase. However, our proposed method can achieve good tracking performance without the need for additional terms, since the dynamics of the output reference is included in the control law. Moreover, the proposed approach does not consider the PV information for real-time implementation, and only an estimate of the term $M(x)b$ is considered to ensure zero steady-state error. As a result, an integral action arises naturally in the controller as it can be shown latter. The disturbance observer proposed in [38] will be used as a basis for further observer design.

3.2 Nonlinear disturbance observer

Define an auxiliary disturbance $\theta \in R^2$ such that

$$\theta = M\left(x\right) b\left(t\right) \tag{20}$$

Note that the nonlinear system is assumed to have a constant steady-state response. Hence, with the assumption in (11), one can assume that the auxiliary disturbance θ is bounded and satisfies

$$\lim_{t\to\infty} \dot{\theta}\left(t\right) = 0 \tag{21}$$

Replacing the term $M(x)b$ by its estimate $\hat{\theta}$, the control law (12) becomes

$$u\left(t\right) = G^{-1}\left(x\right)\left(-\begin{bmatrix} L_f h_1\left(x\right) \\ L_f^2 h_2\left(x\right) \end{bmatrix} - \hat{\theta}\left(t\right) + \begin{bmatrix} r_1 \\ r_2 \end{bmatrix}\right) \tag{22}$$

The nonlinear function $M(x)$ defined in (13) can be rewritten as follows

$$M\left(x\right) = l\left(x\right) g_2 \tag{23}$$

where $l(x)$ is a nonlinear function, and it is given by

$$l\left(x\right) = \begin{bmatrix} \frac{\partial h_1(x)}{\partial x} \\ K_{12}\frac{\partial h_2(x)}{\partial x} + \frac{\partial L_f h_2(x)}{\partial x} \end{bmatrix} \tag{24}$$

Using the above equation, one can show that

$$l\left(x\right) g_1 = G\left(x\right) \tag{25}$$

Combining (23) and (25) with the model given in (4) yields

$$l(x)\dot{x} = l(x)f(x) + G(x)u(t) + \theta(t) \tag{26}$$

As a consequence, the auxiliary disturbance θ in (26), can be estimated by the nonlinear disturbance observer (NDO) [38]

$$\dot{\hat{\theta}}(t) = -\mu\hat{\theta} + \mu\left(l(x)\dot{x} - l(x)f(x) - G(x)u(t)\right) \tag{27}$$

where μ is a constant observer gain to be determined. Thus, the dynamics of the observer error $e_\theta(t) = \hat{\theta}(t) - \theta(t)$ is governed by

$$\dot{e}_\theta = -\mu e_\theta - \dot{\theta} \tag{28}$$

Therefore, with the assumption in (21), it can be shown that the disturbance estimation $\hat{\theta}$ converges to the actual disturbance θ as $t \to \infty$ by choosing

$$\mu = diag\{\mu_1, \mu_2\} \tag{29}$$

where $\mu_{1,2} > 0$. More specifically, the convergence rate of the disturbance observer depends on the choice of μ. As the time derivative of the state is not available, it is essential to further simplify the disturbance observer (27) to make it convenient for practical implementation. In fact, note that

$$\begin{cases} l(x)\dot{x} = \begin{bmatrix} \frac{\partial h_1(x)}{\partial t} & \frac{K_{12}h_2(x)}{\partial t} + \frac{\partial L_f h_2(x)}{\partial t} \end{bmatrix}^T \\ l(x)f(x) = \begin{bmatrix} L_f h_1(x) & K_{12}L_f h_1(x) + L_f^2 h_2(x) \end{bmatrix}^T \end{cases} \tag{30}$$

Hence, substituting the control law (22) into (27), and using (30), then after integration gives the simplified disturbance observer as follows

$$\hat{\theta}(t) = -\mu \begin{pmatrix} K_{01}\int_0^t e_1 d\tau + e_1 \\ K_{02}\int_0^t e_2 d\tau + K_{12}e_2 + (\dot{y}_{r2} - L_f h_2(x)) \end{pmatrix} \tag{31}$$

Thereby, the simplified disturbance observer-based control for the system output y_1 appears as a simple PI controller. For the system output y_2, the observer behaves as a PID controller where the time derivative of the output is replaced by its Lie derivative. The major advantage of the proposed disturbance observer is that its structure is quite convenient for practical implementation, and the disturbance rejection response can be specified by adjusting the observer gain μ.

3.3 Closed-loop stability of the composite controller

In order to investigate the closed-loop stability under the proposed controller, one can further simplify the composite controller by substituting (14) and (31) into the control law (22), which gives

$$u = G^{-1}\begin{bmatrix} I_1\int_0^t e_1 d\tau + P_1 e_1 + N_1(x) \\ I_2\int_0^t e_2 d\tau + P_2 e_2 + D_2(\dot{y}_{r2} - L_f h_2(x)) + N_2(x) \end{bmatrix} \tag{32}$$

where

$$\begin{cases} I_1 = \mu_1 K_{01}, \;\; P_1 = (K_{01} + \mu_1) \\ I_2 = \mu_2 K_{02}, \;\; P_2 = (K_{02} + \mu_2 K_{12}), \;\; D_2 = (K_{12} + \mu_2) \end{cases} \tag{33}$$

and

$$\begin{cases} N_1(x) = (\dot{y}_{r1} - L_f h_1(x)) \\ N_2(x) = \left(\ddot{y}_{r2} - L_f^2 h_2(x)\right) \end{cases} \tag{34}$$

Clearly the resulting control is equivalent to feedback linearization with integral action, but the design method is different. For real-time implementation, the composite controller can be viewed as a PI/almost PID controller with a compensation term $N_{1,2}(x)$. The term 'almost' is due the use of Lie derivative instead of the time derivative of the system output. The main result concerning the closed-loop stability under the controller (32) is stated in the following theorem.

Theorem 3.2. *Consider the nonlinear system (4) for a grid-connected PV system, and suppose that the disturbance $b(t)$ is bounded and satisfies the assumption (3). Then, under the control law (32), the output of the system tracks the desired output with an error which converges to zero as time goes to infinity, i.e.,*

$$\lim_{t\to\infty} e_1(t) = 0, \quad \lim_{t\to\infty} e_2(t) = 0 \tag{35}$$

and the eigenvalues associated with the closed-loop system are given by

$$\lambda_{01} = -\frac{3}{2\varepsilon_i}, \quad \lambda_{11} = -\mu_1 \tag{36}$$

and

$$\lambda_{02} = \frac{-5 \pm j5.32}{4\varepsilon_v}, \quad \lambda_{12} = -\mu_2 \tag{37}$$

With the assumption that the disturbance is bounded and the composite controller contains an integral action, the result is established using input-to-state stability (ISS) theory and the Barbalat's lemma [37] (see Appendix B).

Following (36)-(37), the control parameters can be chosen according to the desired closed-loop performances. Alternatively, the parameter $\varepsilon_{i,v}$ can be chosen as small as possible to achieve good tracking performance. The observer gains $\mu_{1,2}$ can be selected as large as possible to ensure a fast disturbance rejection. However, the selection of such parameters should be made in a tradeoff between fast disturbance estimation and measurement noise attenuation. An implementation process on how to practically apply the proposed controller to the grid-connected PV system is given in Fig. 3(a).

4 Computer Simulations

4.1 Control loop diagram

A detailed block diagram of the proposed approach is depicted in Fig. 3(b). The control inputs v_d and v_q, produced by the proposed controller, are transformed into three-phase voltage commands v_a^*, v_b^*, and v_c^* using $dq - abc$ transformation. Then, the third harmonic injection PWM approach is used to realize the three-phase voltage commands. The main problem associated with the proposed controller is that the d-axis component may exceed its maximum value during transients because of rapid changes in DC-link voltage reference. To overcome such a problem, a limiter is introduced on the set-point changes so that the current will never go

above its limiting value during transients. A PI controller is also designed to control the duty-cycle d of the boost converter so that the PV voltage is regulated to track the desired power point. The design of the PI controller is not described here, as it is beyond the scope of this paper. To evaluate the performances of the proposed controller under a realistic scenario, the photovoltaic power profile is chosen to mimic a real P-V characteristic as shown in Fig. 4. This is done by using the PV panel model developed in [39].

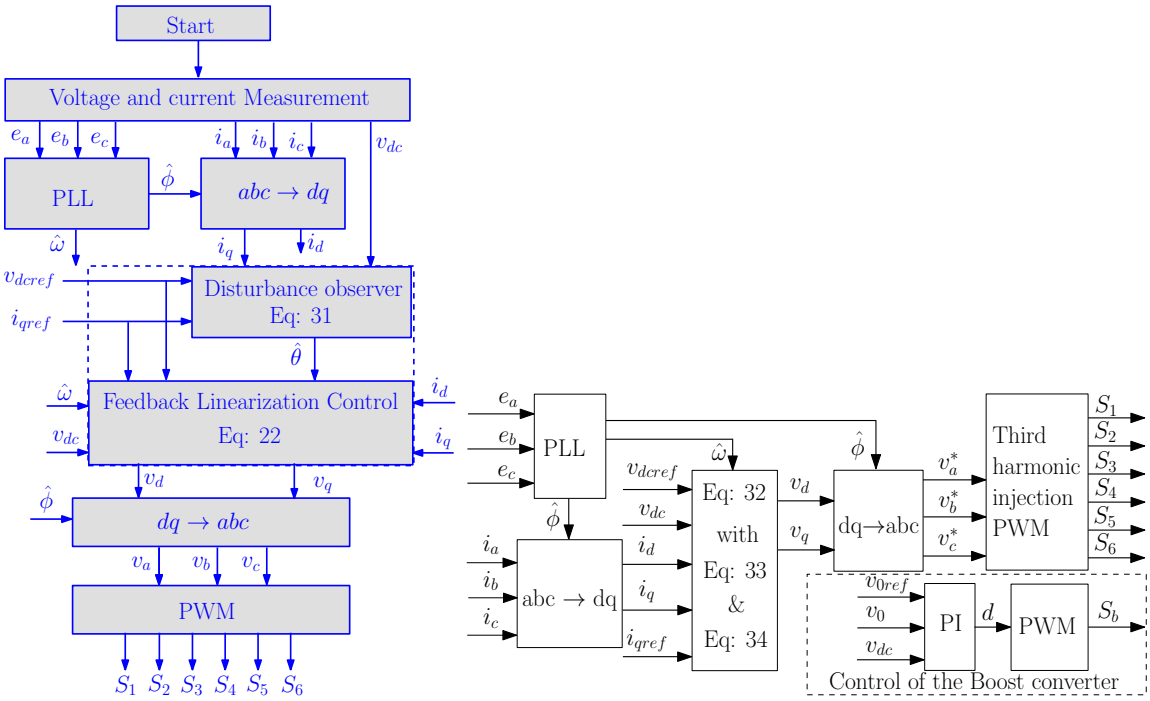

(a) Implementation process of the proposed controller

(b) Control loop diagram of a grid-connected PV inverter system including the control of the boost converter.

Fig. 3 Flowchart and block diagram for applying the proposed controller to a grid-connected PV inverter system.

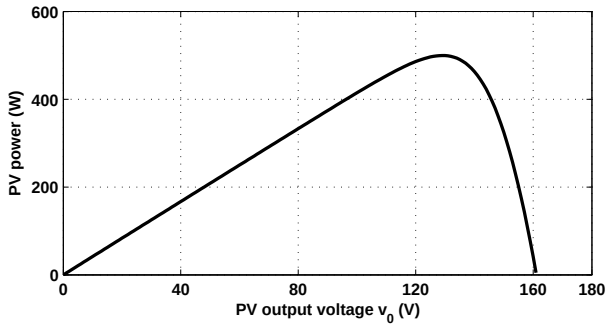

Fig. 4 P-V characteristic.

4.2 Simulation Results

To evaluate the effectiveness of the proposed method, a computer simulations have been carried out using Matlab/Simulink software package, where the sampling time for the mathematical model of the complete

system is fixed to 0.001 ms. The control period is set equal to 0.1 ms, while the switching frequency of the PWM signal is chosen equal to 5 kHz. The parameters of the controller can be determined based on the desired specifications of the closed-loop system. In this work, the parameters $(\varepsilon_i, \varepsilon_v)$ associated with the controller gains are set to (0.001, 0.01) while the observer gains (μ_1, μ_2) are set equal to (16.6, 25). The controller parameters are designed so that the current control loop has much faster response than that of the DC-link voltage control loop. The set-point of the DC-link voltage is set equal to 200 V, and the q-axis current reference is chosen equal to zero in order to ensure unity power factor operation. Fig. 5(a)–(b) shows the steady-state and transient performances of the feedback linearization-based control with and without a disturbance observer. During the startup phase, the dc-dc boost converter is disconnected from the grid-side converter, and only nominal parameters are considered in both controllers. At t = 0.6 s, both converters are interconnected, and the PV power was stepped up from zero to 500 W by adjusting the PV output voltage v_0. From the results, it can be seen that the use of the disturbance observer guarantees zero steady-state error despite the presence of unknown unmatched disturbance i_0. However, an offset is observed when the disturbance observer is not incorporated in the control law even if no uncertainty/disturbance is considered during the startup phase. This explains why a disturbance observer is necessary even if the model can be accurately determined.

Figure 5(c)–(d) compares the performances of the proposed controller with that obtained with an existing PV control technique [20], inspired from feedback linearization theory and denoted here by $\text{FLC}_{1,2}$. The subscript 1 is refereed to the case where both the proposed approach and the controller FLC have the same controller gains K_{01}, K_{02} and K_{12} to guarantee a fair comparison. For FLC_2, the controller gains are determined by setting $\alpha_{01} = 1$, $\alpha_{02} = 1$, and $\alpha_{12} = 2$ as in [20]. The integral coefficients for $\text{FLC}_{1,2}$ approach are chosen to be equal to that used for the proposed controller so as to have a fair comparison in terms of disturbance rejection capability. As seen, all the controllers have proved to be effective in terms of eliminating the steady-state error because of the existence of integral action, however, a large DC-link voltage tracking error is observed with FLC method during the startup stage. Moreover, it can be observed that the proposed approach exhibits better disturbance rejection performance in comparison with FLC_2. It can also be seen that the q-axis current is well controlled with the proposed approach. As pointed out in [20], the startup dynamic performance can be improved by designing a smoothing term to be combined with FLC. However, such a requirement will further complicate the design process.

5 Experimental Results

5.1 Laboratory Test Setup

The proposed control scheme for a grid-interconnected photovoltaic inverter is implemented in real-time on a three-leg IGBT-based two level inverter using the DS1103 board. The laboratory test bed consists of two DC-link capacitors connected in series, three-phase IGBT with drivers, a line filter, and a step up transformer which connects the system to the power grid. To consider the real dynamics of the PV system, the P-V characteristic, shown in Fig. 4, is generated using a 2 kW PV emulator connected to a DC-link via dc-dc converter. This test bed setup is depicted in Fig. 6. The system parameters are given in Table I of the Appendix C. For the system

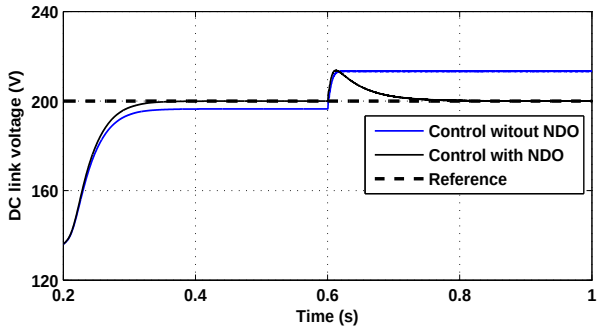

(a) DC-link voltage response.

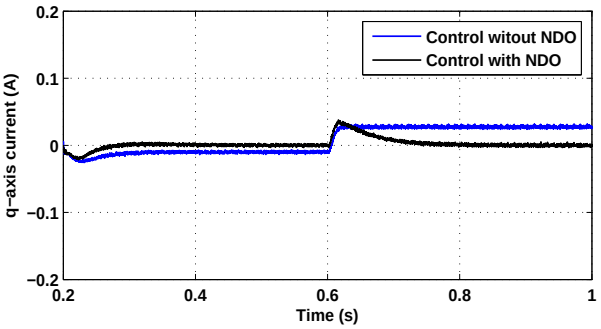

(b) q-axis current response.

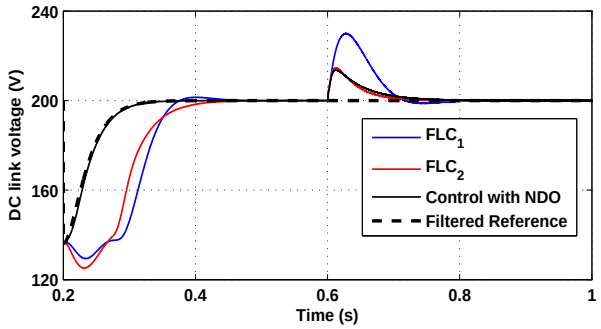

(c) DC-link voltage response.

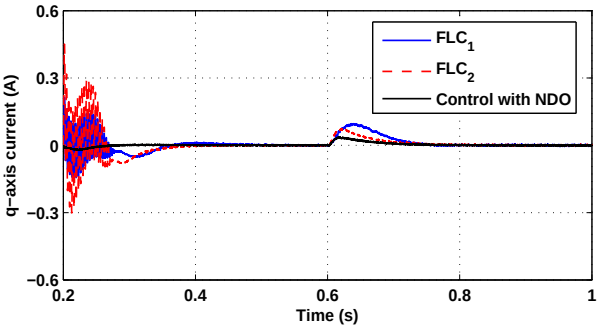

(d) q-axis current response.

Fig. 5 system's response under feedback linearization-based control with and without NDO.

design, it is noticed that the parameters of the L filter are imposed by the experimental setup. The grid voltage amplitude is chosen so that the inverter modulation index cannot go above the unity for the given experimental

setup. Then, a three-phase transformer is placed between the main grid and the line filter to realize the desired grid voltage amplitude. The DS1103 board is used in this experiment to control the boost converter and the grid-tied inverter. It is equipped with Power PC 750GX (Master processor) running at 1 GHz, and a Texas Instruments TMS320F240 DSP (slave processor) running at 20 MHz.

In order to show, practically, the effectiveness of the proposed approach in controlling a grid-connected PV system, two scenarios were performed experimentally. For such tests, the control period, the switching frequency and the parameters of the controller are chosen similar to those used for the simulation test.

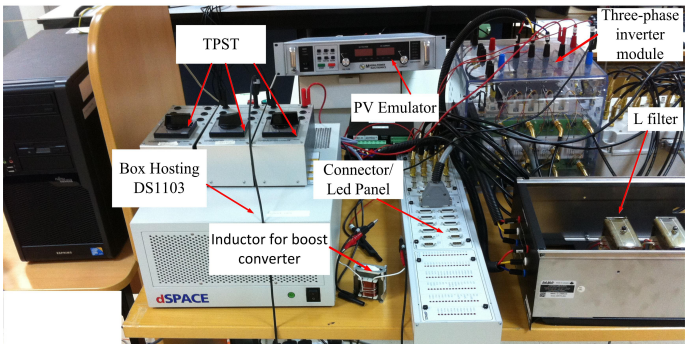

Fig. 6 Block diagram of the proposed approach scheme for a grid-connected PV inverter system.

5.2 Performance Evaluation under Normal Operation and Model Uncertainty

The main objective of this experiment is to test the closed-loop system under a sudden change in the PV output voltage. This scenario may arise when the voltage reference v_{0ref}, for the PI controller, is generated by a maximum power point tracking algorithm. Initially, the PV system was operating at a low power and at t = 0.4 s, the PV output voltage reference was suddenly stepped down from 155 to 130 V and then back to 155 V at t = 1.4 s, which corresponds to a PV output power step of 300 W. The voltage reference v_{0ref} is fed to the PI controller to adjust the switch duty-ratio of the boost converter so as to regulate the PV output voltage v_0 to its reference. It is noted that the PI controller parameters are tuned so that the PV output voltage v_0 reaches its reference v_{0ref} within 15 ms, which is fast enough to verify the disturbance rejection capability of the proposed system. Additionally, the capacitance C and the inductance L, used in the controller, were set equal to 50% of their actual values with the aim of testing the robustness of the proposed controller. As shown in Fig. 7(a), it is clear that the proposed controller reacts in a quick manner, and the steady-state error is removed quickly after changes in power. Fig. 7(b) represents the three-phase line current at the maximum power point, and it can be observed that the system can operate at a low total harmonic distortion of the current.

5.3 Performance Evaluation under Reactive Power Changes and Model Uncertainty

This test was performed to verify the control performance under a step change in reactive power. This scenario may arise when PV plant is required to respond to the grid operator request, to maintain certain voltage level

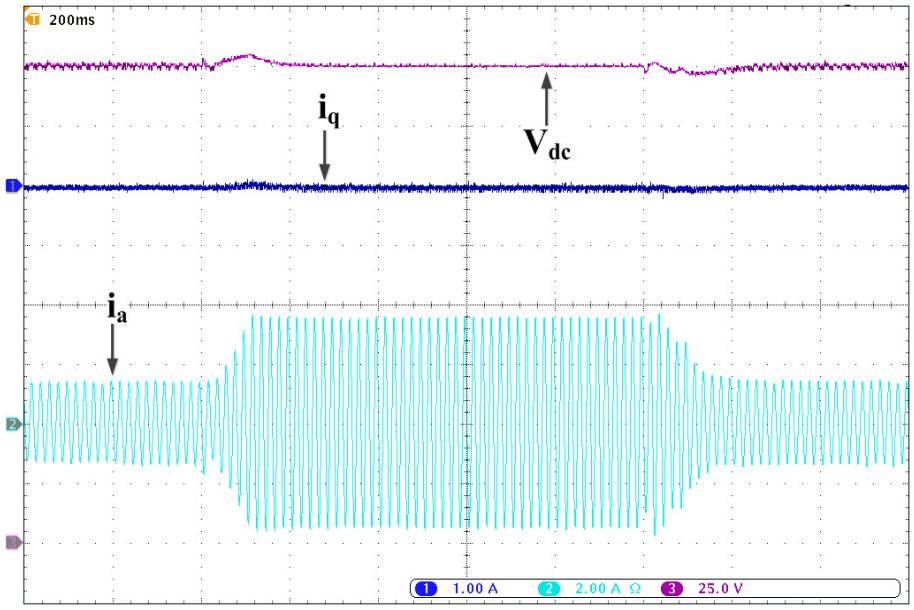

(a) Phase current i_a (2), DC-link voltage (3), and q-axis current (1).

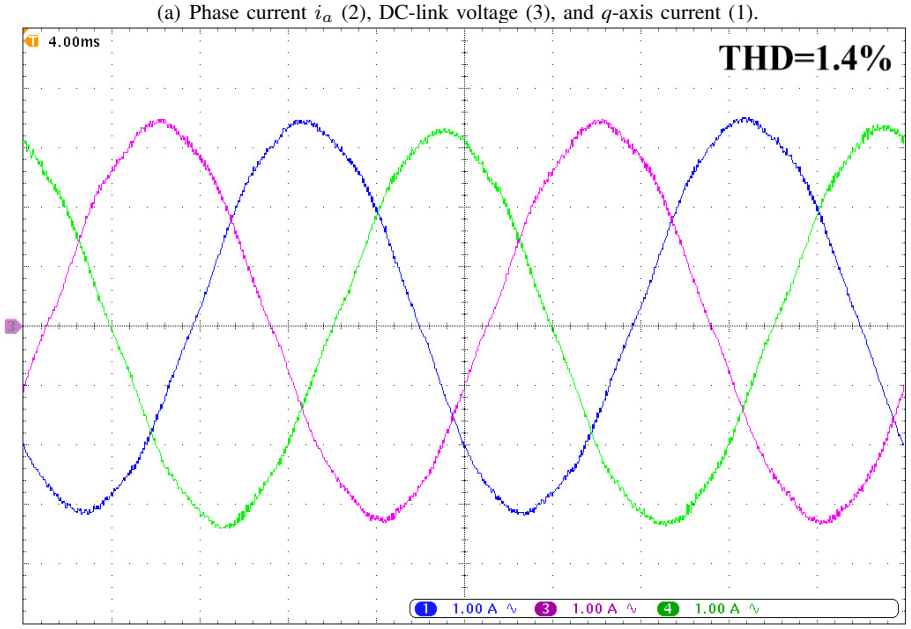

(b) Three phase line current.

Fig. 7 System's response under the proposed controller.

due to a change in operating conditions such as switching on big loads, loss of distribution feeder, etc. This can be accomplished by investigating the performances of the closed-loop system under a step change in q-axis current reference. Moreover, the capacitance C and the inductance L, used in the controller, were increased by 50% in comparison with the actual values. As shown in Fig. 8, the q-axis current reference was stepped down to -1 A, and then returned back to 0 A after 80 ms. It is noticed that the q-axis current is chosen negative because the reactive power Q, injected into the grid, is expressed as $Q = -1.5 e_d i_q$. From the results, it can be observed that the q-axis current reaches its steady-state value within a few milliseconds, which is consistent

with the design of the controller parameters. It can also be observed that the DC-link voltage regulation is almost insensible to the reactive power change, and the unity power factor operation is guaranteed during the period when the reactive power is null. Here, the PV power was kept constant and set to 170 W by maintaining the PV output voltage equal to 156 V.

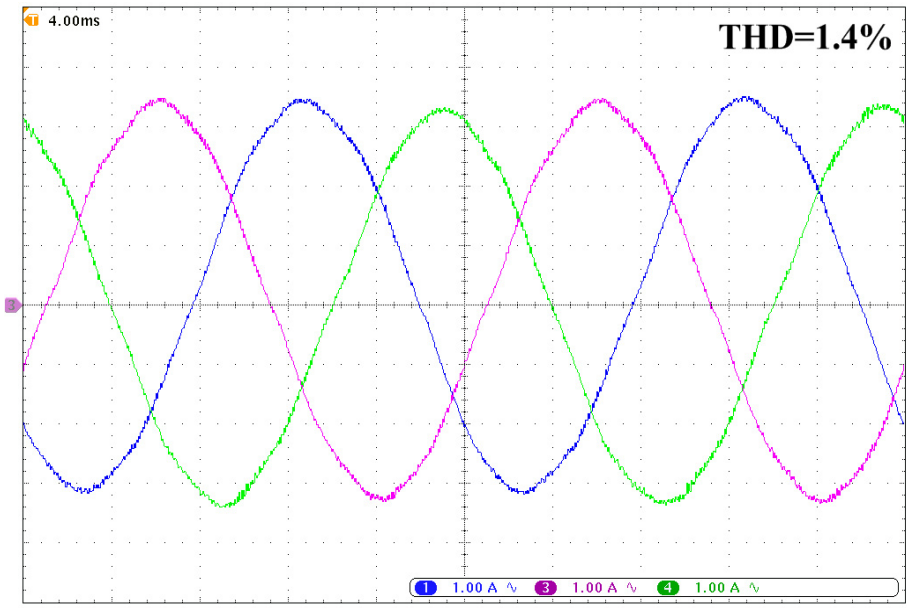

Fig. 8 Phase current i_a (2), grid voltage e_a (4), DC-link voltage (3), and q-axis current (1).

6 Conclusions

This paper has presented an exact feedback linearization-based control for a grid-connected PV inverter. The elimination of the steady-state error represents a major objective of the proposed approach. For this, a PI/almost PID disturbance observer is derived based on a newly defined design function vector. As a result, the resulting disturbance observer is asymptotically stable, and easy to implement in a real-time system without resorting to integrate the high-order nonlinear system model. This is due to the fact that the resulting disturbance observer relies only on the reference, its time derivative, and the Lie derivative of the output, whilst the case of the existing disturbance observer-based control, the estimate of the unmatched disturbance is driven by integrating a nonlinear system model. The effectiveness of the proposed approach is illustrated by both simulation and experimental results under modeling errors and external unknown disturbances. The proposed method can be considered as an alternative approach in improving disturbance attenuation ability and performance robustness for a grid-connected PV inverter under a wide range of disturbances. The method is equally applicable for other renewable energy applications. In our future work, we endeavor to adapt the proposed disturbance observer so as to compensate time-varying disturbance, with a known and fixed frequency. Such a methodology allows improving the steady-state performance of grid-connected PV systems under unbalanced and distorted grid voltage, which is considered as an open research filed.

Acknowledgment

This work was supported by "The Petroleum Institute Research Center (PIRC)" Research Grant.

7 References

1 Yang, F., Yang, L., and Ma, X.: 'An advanced control strategy of pv system for low-voltage ride-through capability enhancement', *Solar Energy*, 2014, **109**, pp. 24–35

2 Lin, F., Lu, K., Ke, T., Yang, B., and Chang, Y.: 'Reactive power control of three-phase grid-connected pv system during grid faults using takagi-sugeno-kang probabilistic fuzzy neural network control', *IEEE Trans. Ind. Electron.*, Sept 2015, **62**, (9), pp. 5516–5528

3 Mahmud, M., Hossain, M., Pota, H., and Roy, N.: 'Robust nonlinear controller design for three-phase grid-connected photovoltaic systems under structured uncertainties', *IEEE Trans. Power. Del.*, June 2014, **29**, (3), pp. 1221–1230

4 Blasko, V. and Kaura, V.: 'A new mathematical model and control of a three-phase ac-dc voltage source converter', *IEEE Trans. Power. Electron.*, 1997, **12**, (1), pp. 116–123

5 Kazmierkowski, M. P. and Malesani, L.: 'Current control techniques for three-phase voltage-source pwm converters: a survey', *IEEE Trans. Ind. Electron.*, 1998, **45**, (5), pp. 691–703

6 Hu, J., Zhu, J., and Dorrell, D. G.: 'Model predictive control of grid-connected inverters for pv systems with flexible power regulation and switching frequency reduction', *IEEE Trans. Ind. Appl.*, 2015, **51**, (1), pp. 587–594

7 Hasanien, H. M. and Muyeen, S.: 'A taguchi approach for optimum design of proportional-integral controllers in cascaded control scheme', *IEEE Trans. Power Sys.*, 2013, **28**, (2), pp. 1636–1644

8 Kato, T., Inoue, K., and Ueda, M.: 'Lyapunov-based digital control of a grid-connected inverter with an lcl filter', *IEEE J. Emerg. Sel. Topics Power Electron.*, 2014, **2**, (4), pp. 942–948

9 Castilla, M., Miret, J., Camacho, A., Matas, J., Vicuna, D., and García, L.: 'Reduction of current harmonic distortion in three-phase grid-connected photovoltaic inverters via resonant current control', *IEEE Trans. Ind. Electron.*, 2013, **60**, (4), pp. 1464–1472

10 Li, P., Yu, X., Zhang, J., and Yin, Z.: 'The h_∞ control method of grid-tied photovoltaic generation', *IEEE Trans. Smart Grid*, July 2015, **6**, (4), pp. 1670–1677

11 Isidori, A.: 'Nonlinear control systems: An introduction(3rd edn)' (Springer-Verlag, 1995)

12 Lalili, D., Mellit, A., Lourci, N., Medjahed, B., and Berkouk, E.: 'Input output feedback linearization control and variable step size mppt algorithm of a grid-connected photovoltaic inverter', *Renew. Energy*, 2011, **36**, (12), pp. 3282–3291

13 Bao, X., Zhuo, F., Tian, Y., and Tan, P.: 'Simplified feedback linearization control of three-phase photovoltaic inverter with an lcl filter', *IEEE Trans. Power Electron.*, June 2013, **28**, (6), pp. 2739–2752

14 Lee, T.-S.: 'Input-output linearization and zero-dynamics control of three-phase ac/dc voltage-source converters', *IEEE Trans. Power Electron.*, Jan 2003, **18**, (1), pp. 11–22

15 Gensior, A., Sira-RamiÂ´rez, H., Rudolph, J., and Guldner, H.: 'On some nonlinear current controllers for three-phase boost rectifiers', *IEEE Trans. Ind. Electron.*, Feb 2009, **56**, (2), pp. 360–370

16 Kim, D.-E. and Lee, D.-C.: 'Feedback linearization control of three-phase ups inverter systems', *IEEE Trans. Ind. Electron.*, March 2010, **57**, (3), pp. 963–968

17 Delfino, F., Denegri, G., Invernizzi, M., and Procopio, R.: 'Feedback linearisation oriented approach to q-v control of grid connected photovoltaic units', *IET Renew. Power Gen.*, Sept 2012, **6**, (5), pp. 324–339

18 Mahmud, M., Pota, H., and Hossain, M.: 'Dynamic stability of three-phase grid-connected photovoltaic system using zero dynamic design approach', *IEEE J. Photovolt.*, Oct 2012, **2**, (4), pp. 564–571

19 Mahmud, M., Pota, H., Hossain, M., and Roy, N.: 'Robust partial feedback linearizing stabilization scheme for three-phase grid-connected photovoltaic systems', *IEEE J. Photovolt*, Jan 2014, **4**, (1)

20 Khajehoddin, S., Karimi-Ghartemani, M., Jain, P., and Bakhshai, A.: 'A control design approach for three-phase grid-connected renewable energy resources', *IEEE Trans. Sustain. Energy*, 2011, **2**, (4), pp. 423–432

21 Wang, C., Li, X., Guo, L., and Li, Y. W.: 'A nonlinear-disturbance-observer-based dc-bus voltage control for a hybrid ac/dc microgrid', *IEEE Trans. Power Electron.*, Nov 2014, **29**, (11), pp. 6162–6177

22 Yang, J., Li, S., and Yu, X.: 'Sliding-mode control for systems with mismatched uncertainties via a disturbance observer', *IEEE Trans. Ind. Electron.*, 2013, **60**, (1), pp. 160–169

23 Ginoya, D., Shendge, P., and Phadke, S.: 'Sliding mode control for mismatched uncertain systems using an extended disturbance observer', *IEEE Trans. Ind. Electron.*, 2014, **61**, (4), pp. 1983–1992

24 Chen, P., Sun, M., Yan, Q., and Fang, X.: 'Adaptive asymptotic rejection of unmatched general periodic disturbances in output-feedback nonlinear systems', *IEEE Trans. Autom. Control*, April 2012, **57**, (4), pp. 1056–1061

25 Ding, Z.: 'Almost disturbance decoupling of uncertain nonlinear output feedback systems', *IEE Proc. Control Theory Appl*, 1999, **146**, (2), pp. 220–226

26 Marino, R. and Tomei, P.: 'Nonlinear output feedback tracking with almost disturbance decoupling', *IEEE Trans. Autom. Control*, 1999, **44**, (1), pp. 18–28

27 Marino, R. and Tomei, P.: 'Adaptive output feedback regulation with almost disturbance decoupling for nonlinearly parameterized systems', *Int. J. Robust Nonlinear Control*, 2000, **10**, (8), pp. 655–669

28 Isidori, A., Schwartz, B., and Tarn, T.: 'Semiglobal l_2 performance bounds for disturbance attenuation in nonlinear systems', *IEEE Trans. Autom. Control*, 1999, **44**, (8), pp. 1535–1545

29 Lin, Z.: 'Almost disturbance decoupling with global asymptotic stability for nonlinear systems with disturbance-affected unstable zero dynamics', *Syst. Control Letters*, 1998, **33**, (3), pp. 163–169

30 Chen, C.-C. and Lin, Y.-F.: 'Application of feedback linearisation to the tracking and almost disturbance decoupling control of multi-input multi-output nonlinear system', *IEE Proc. Control Theory Appl*, 2006, **153**, (3), pp. 331–341

31 Yang, J., Chen, W.-H., Li, S., and Chen, X.: 'Static disturbance-to-output decoupling for nonlinear systems with arbitrary disturbance relative degree', *Int. J. Robust Nonlinear Control*, 2013, **23**, (5), pp. 562–577

32 Li, S., Yang, J., Chen, W.-H., and Chen, X.: 'Disturbance observer-based control: methods and applications' (CRC press, 2014)

33 Chen, W.-H., Yang, J., Guo, L., and Li, S.: 'Disturbance-observer-based control and related methods: An overview', *IEEE Trans. Ind. Electron.*, 2016, **63**, (2), pp. 1083–1095

34 Yang, J. and Zheng, W. X.: 'Offset-free nonlinear mpc for mismatched disturbance attenuation with application to a static var compensator', *IEEE Trans. Circuits Syst. II: Express Briefs*, Jan 2014, **61**, (1), pp. 49–53

35 Yang, J., Zheng, W., Li, S., Wu, B., and Cheng, M.: 'Design of a prediction accuracy enhanced continuous-time mpc for disturbed systems via a disturbance observer', *IEEE Trans. Ind. Electron.*, 2015, **62**, (9), pp. 5807–5816

36 Chung, S.-K.: 'A phase tracking system for three phase utility interface inverters', *IEEE Trans. Power Electron.*, 2000, **15**, (3), pp. 431–438

37 Khalil, H. K.: 'Nonlinear systems' (Prentice hall Upper Saddle River, 2002), **3**

38 Chen, W.-H.: 'Disturbance observer based control for nonlinear systems', *IEEE/ASME Trans. Mechatronics*, 2004, **9**, (4), pp. 706–710

39 Villalva, M., Gazoli, J., and Filho, E.: 'Comprehensive approach to modeling and simulation of photovoltaic arrays', *IEEE Trans. Power Electron.*, 2009, **24**, (5), pp. 1198–1208

8 Appendices

8.1 Lie derivative

$$L_f h(x) = \frac{\partial h}{\partial x} f,\ L_{g_{1,2}} h(x) = \frac{\partial h}{\partial x} g_{1,2} \tag{38}$$

$$L_f^2 h(x) = \frac{\partial L_f h(x)}{\partial x} f,\ L_{g_{1,2}} L_f h(x) = \frac{\partial L_f h(x)}{\partial x} g_{1,2} \tag{39}$$

8.2 Proof of theorem 3.2

By substituting the control law (32) into (9)- (10), the dynamic errors of the closed-loop system can be expressed as follows

$$\dot{e}_1 + (\mu_1 + K_{01}) e_1 + \mu_1 K_{01} \int_0^t e_1 d\tau = -\frac{b_q}{L} \tag{40}$$

and

$$\ddot{e}_2 + (\mu_2 + K_{12}) \dot{e}_1 + (\mu_2 K_{12} + K_{02}) e_2 + \mu_2 K_{02} \int_0^t e_2 d\tau = \delta(t) \tag{41}$$

where

$$\delta(t) = -\left(K_{12} + \mu_2 + \frac{3e_d}{2Cv_{dc}^2} i_d\right) \frac{b_v}{C} - \frac{\dot{b}_v}{C} + \frac{3e_d b_d}{2CLv_{dc}} \tag{42}$$

Let $\varepsilon = \begin{bmatrix} e_1 & \sigma_1 \end{bmatrix}^T$ and $\eta = \begin{bmatrix} e_2 & \dot{e}_2 & \sigma_2 \end{bmatrix}$ be the new coordinates, with

$$\sigma_1 = \int_0^t e_1 d\tau,\ \sigma_2 = \int_0^t e_2 d\tau \tag{43}$$

Then, the equations (40)-(41) can be rewritten in the new (ε, η) coordinates as

$$\begin{cases} \dot{\varepsilon} = A_1 \varepsilon + \Delta_1(t) \\ \dot{\eta} = A_2 \eta + \Delta_2(t) \end{cases} \tag{44}$$

where A_1 and Δ_1 are given by

$$A_1 = \begin{bmatrix} -(\mu_1 + K_{01}) & -\mu_1 K_{01} \\ 1 & 0 \end{bmatrix},\ \Delta_1(t) = \begin{bmatrix} -\frac{b_q}{L} \\ 0 \end{bmatrix} \tag{45}$$

The matrix A_2 is expressed as follows

$$A_2 = \begin{bmatrix} 0 & 1 & 0 \\ -(\mu_2 K_{12} + K_{02}) & -(\mu_2 + K_{12}) & -\mu_2 K_{02} \\ 1 & 0 & 0 \end{bmatrix} \tag{46}$$

The vector Δ_2 is given by

$$\Delta_2(t) = \begin{bmatrix} 0 \\ \delta(t) \\ 0 \end{bmatrix} \tag{47}$$

The eigenvalues associated with the closed-loop system are those of A_1 and A_2. By considering (17) and (19), the eigenvalue of the matrix A_1 are

$$\lambda_{01} = -\frac{3}{2\varepsilon_i},\quad \lambda_{11} = -\mu_1 \tag{48}$$

and those of matrix A_2 are

$$\lambda_{02} = \frac{-5 \pm j5.32}{4\varepsilon_v},\quad \lambda_{12} = -\mu_2 \tag{49}$$

As all the eigenvalues have negative real parts, A_1 and A_2 are Hurwitz matrices.

Input-to-state stability (ISS) presented in [37] states that if A_i is Hurwitz matrix, the trajectory ε, respectively η, is bounded for every bounded input disturbance Δ_i. Therefore, with the assumption that b_q is bounded, ISS allows to conclude that the trajectory ε is bounded. This means that $\sigma_1$defined by 43 is bounded.

The Barbalat's lemma presented in [37] states that if $\psi : R \to R$ is uniformly continuous function on $[0, \infty)$, and

$$\lim_{t\to\infty} \int_0^\tau \psi(\tau)\, d\tau \tag{50}$$

exists and is finite, then $\psi(t) \to 0$ as $t \to \infty$. As the nonlinear system under investigation is continuous, and all the input signals are continuous, the error signal e_1, is continuous. By the fact that σ_1 is bounded and continuous, the Barbalat's lemma allows to conclude that

$$\lim_{t\to\infty} e_1(t) = 0 \tag{51}$$

Regarding the subsystem η, it follows from (2)that

$$\frac{3e_d}{2Cv_{dc}^2} i_d = \frac{1}{v_{dc}} \left(\dot{v}_{dc} - \frac{b_v}{C} \right) \tag{52}$$

Then, one can write

$$\begin{cases} v_{dc} = v_{dcref} - e_2 \\ \frac{3e_d}{2Cv_{dc}^2} i_d = \frac{1}{(v_{dcref} - e_2)} \left(\frac{b_v}{C} - (\dot{v}_{dcref} - \dot{e}_2) \right) \end{cases} \tag{53}$$

By substituting (53) into $\delta(t)$ in (42), it can be shown that $\Delta_2(t)$ is bounded and its bound $\bar{\Delta}_2$ only depends on errors e_2, $\dot{e}_2$, and references v_{dcref}, and $\dot{v}_{dcref}$ but not on σ_2. Under this condition, one can write

$$\|\Delta_2(t)\| \leq \bar{\Delta}_2 \left(\|e_2\|, \|\dot{e}_2\|, \|v_{dcref}\|, \|\dot{v}_{dcref}\| \right) \tag{54}$$

As the matrix A_2 is Hurwitz, then, there exist symmetric and positive-definite matrices P and Q, such that

$$A_2^T P + P A_2 = -Q \tag{55}$$

Now, let $V(\eta)$ be the Lyapunov function candidate for the subsystem η, where

$$V(\eta) = \eta^T P \eta \tag{56}$$

Differentiating the Lyapunov function candidate V along the trajectories of (44) gives

$$\begin{aligned} \dot{V}(\eta) &= -\eta^T Q \eta + 2\eta^T P \Delta_2(t) \\ &\leq -\|\eta\|^2 \left(\lambda_{\min}(Q) - \frac{2\lambda_{\max}(P)\|\Delta_2(t)\|}{\|\eta\|} \right) \end{aligned} \tag{57}$$

where $\lambda_{min}(X)$ and $\lambda_{max}(X)$ represent the minimum and the maximum eigenvalues of a matrix X, respectively. It follows from (57), that a sufficient condition for the time derivative of $V(\eta)$ being negative is

$$\|\eta\| = \sqrt{e_2^2 + \dot{e}_2^2 + \sigma_2^2} \geq \frac{2\lambda_{\max}(P)}{\lambda_{\min}(Q)} \|\Delta_2(t)\| \tag{58}$$

With the assumption that the disturbance Δ_2 is bounded, and its bound does not depend on σ_2, one can use theorem 4.19 in [37] to show that the subsystem η is ISS. This means that σ_2 is bounded. By considering the continuity of e_2 and the definition of σ_2, the Barbalat's lemma yields

$$\lim_{t \to \infty} e_2(t) = 0 \tag{59}$$

8.3 Parameters of the grid-interlinked PV inverter

The parameter values of the grid-interlinked PV inverter system are summarized in Table I.

Table 1: Parameters of the grid-interlinked PV inverter

Maximum power of PV unit (W)	500
DC link voltage (V)	200
Line-to-line grid voltage (V)	100
Inverter inductance (mH)	52
DC link capacitor (mF)	1.052
Boost inductance (mH)	5
Frequency (Hz)	50